

Vortex nucleation in Bose-Einstein condensates in time-dependent traps

Emil Lundh,^{1,*} J.-P. Martikainen,^{1,2,3} and Kalle-Antti Suominen^{1,3}

¹Helsinki Institute of Physics, PL 64,

FIN-00014 Helsingin yliopisto, Finland

²Institute for Theoretical Physics, Utrecht University,

Leuvenlaan 4, 3584 CE Utrecht, The Netherlands

³Department of Physics, University of Turku,

FIN-20014 Turun yliopisto, Finland

(Dated: November 7, 2018)

Abstract

Vortex nucleation in a Bose-Einstein condensate subject to a stirring potential is studied numerically using the zero-temperature, two-dimensional Gross-Pitaevskii equation. In the case of a rotating, slightly anisotropic harmonic potential, the numerical results reproduce experimental findings, thereby showing that finite temperatures are not necessary for vortex excitation below the quadrupole frequency. In the case of a condensate subject to stirring by a narrow rotating potential, the process of vortex excitation is described by a classical model that treats the multitude of vortices created by the stirrer as a continuously distributed vorticity at the center of the cloud, but retains a potential flow pattern at large distances from the center.

*Electronic address: Emil.Lundh@helsinki.fi

I. INTRODUCTION

Since the first experimental creation of a quantized vortex in a gaseous Bose-Einstein condensate (BEC) [1, 2], there has been significant experimental and theoretical advance in this field of research. However, even in these relatively simple systems, the understanding of such a basic issue as the mechanism for nucleation of vortices has not been straightforward.

Several experimental methods of vortex creation are currently in use, including phase imprinting [1, 3], cooling of a rotating normal gas [4], and conversion of spin angular momentum into orbital angular momentum by reversal of the magnetic bias field in a Ioffe-Pritchard trap [5, 6, 7]. The topic of this paper is the mechanical stirring of a Bose-Einstein condensed cloud with the use of optical and magnetic fields. This method, in turn, falls into two categories: rotation of an anisotropic trap and stirring with a narrow potential, and we shall examine each of those in turn.

References [2, 8] reported on vortex creation in gases that are confined in traps whose equipotential curves in the x - y plane have a slightly elliptic shape and are varied in time so that the axis of ellipticity rotates around the third axis. The formation of vortices in such traps is understood to be a consequence of the excitation of unstable quadrupole modes [9, 10]. Accordingly, vortices are seen to occur first when the angular frequency of rotation is in the vicinity of $1/\sqrt{2}$ times the average radial trapping frequency ω (that is, the frequency of the quadrupole mode divided by its angular-momentum quantum number) [8, 11]. However, the range of parameter values within which vortices are experimentally seen to be created is not yet entirely accounted for by theory. This shall be discussed in detail later.

Finally, vortices can be excited by the use of a repulsive optical potential which is confined to a small region of the plane, thus mimicking a stick which is moved through the gas cloud in order to stir up vortices [12]. In this kind of geometry, local turbulence including the creation of vortex-antivortex pairs at the position of the stirrer is instrumental in inducing angular momentum in the gas [13].

In this paper, we set out to investigate to what extent the experimental findings can be accounted for by two-dimensional zero-temperature theory. We shall do so with means of numerical calculations and, when possible, classical hydrodynamical modelling. The paper is organized as follows. The equation of motion, the numerical methods and the elements of

the theoretical understanding of vortex nucleation are introduced in Section II. In Sec. III we study the formation of vortices in a rotating elliptical trap and compare our numerics with the experimental findings. Section IV is concerned with the method of stirring the gas with a moving narrow optical potential. In Sec. V we summarize and conclude.

II. EQUATIONS AND NUMERICAL METHOD

We assume the gas cloud to be at sufficiently low temperature and low density that it can be described as a pure condensate. Such a system is entirely governed by a scalar condensate wave function $\psi(\mathbf{r}, t)$ that evolves in time according to the Gross-Pitaevskii equation [14, 15]:

$$i\hbar \frac{\partial \psi}{\partial t} = -\frac{\hbar^2}{2m} \nabla^2 \psi + V(\mathbf{r}, t) \psi + \frac{4\pi\hbar^2 a}{m} |\psi|^2 \psi. \quad (1)$$

The local fluid density and velocity are given in terms of the condensate wave function by $n(\mathbf{r}, t) = |\psi(\mathbf{r}, t)|^2$ and $\mathbf{v}(\mathbf{r}, t) = (\hbar/m) \nabla(\arg \psi(\mathbf{r}, t))$. The nonlinear term in Eq. (1) describes inter-particle interactions in the s-wave approximation and its strength is determined by the s-wave scattering length a . $V(\mathbf{r}, t)$ represents the external potential and can in experiments be of both magnetic and optical origin. We shall in the following take $V(\mathbf{r}, t)$ to be the sum of two terms, a two-dimensional cylindrically symmetric harmonic-oscillator potential and an asymmetric time-dependent term:

$$V(x, y, t) = \frac{1}{2} m \omega^2 (x^2 + y^2) + \Delta V(x, y, t). \quad (2)$$

The spatial extent of the one-particle ground state of the harmonic potential is called the oscillator length, $a_{\text{osc}} = (\hbar/m\omega)^{1/2}$. Finally, the condensate wave function ψ is in two dimensions normalized to the number of particles per unit length which we denote N/l_z , so that l_z is the average extent of the cloud in the z direction.

We shall make frequent use of the Thomas-Fermi approximation, which neglects the kinetic term in the Gross-Pitaevskii equation [16]. This approximation gives an accurate description of the bulk properties of the cloud when the coupling is strong; however, it fails to correctly describe short-range density variations such as that at the cloud boundary and close to a vortex core. The stationary-state density in the Thomas-Fermi approximation, assuming an isotropic harmonic-oscillator potential, is

$$n(r) = n_0 \left(1 - \frac{r^2}{R_{\text{TF}}^2} \right) \quad (3)$$

in the region where the right-hand side is positive and zero elsewhere. The central density is given by $n_0 = \mu m / (4\pi\hbar^2 a)$; the chemical potential μ is determined by normalization. In the two-dimensional case considered here, $\mu = 2\hbar\omega\sqrt{Na/l_z}$. The Thomas-Fermi cloud radius is $R_{\text{TF}} = 2(Na/l_z)^{1/4}a_{\text{osc}}$. Of importance is also the healing length ξ , which determines the size of a vortex core; in the Thomas-Fermi approximation it is given by $\xi = (a_{\text{osc}}/R_{\text{TF}})a_{\text{osc}}$. The condition of strong coupling is fulfilled when $R_{\text{TF}} \gg \xi$ or, equivalently, when the coupling parameter Na/l_z is large.

In the numerical study, the Gross-Pitaevskii equation (1) is propagated in real time in the nonrotating (laboratory) reference frame, subject to an explicitly time-dependent potential, using the split-step Fourier method. We have chosen not to use any phenomenological model for finite-temperature dissipation such as an imaginary component in the time step (cf. [17, 18, 19]).

As already mentioned above, we have chosen to study only two-dimensional systems, knowing that the physics of vortex formation for oblate systems will be well described by such a model. In fact, as we shall see, the model seems to be able to describe with limited accuracy the essential physics of vortex formation also for a prolate system.

During the temporal evolution, we have, in addition to the complex wave function itself, monitored the total angular momentum, the mean extension of the cloud along suitably chosen axes (corotating with the disturbance) and the total fluid circulation within a region close to the condensate center. All these quantities are measurable experimentally, and we shall see that each of them exhibits a clear signal in its time evolution when vortices enter the interior of the cloud.

For a vortex to be created, it must be energetically favorable compared with a nonrotating state [20], but in addition, there must be a dynamical instability of the cloud that permits vortex creation. Generally, an excitation can only be created due to a moving disturbance in the fluid when the velocity exceeds a critical one, given by the Landau criterion [21]:

$$v_c = \min_q \frac{E_q}{q}, \quad (4)$$

where q denotes the wave numbers of all possible quasiparticle modes. For a trapped BEC subject to a rotating perturbation close to the condensate edge, the Landau analysis yields a critical angular velocity in terms of the surface modes [9, 22]:

$$\Omega_c = \min_l \frac{\omega_l}{l}, \quad (5)$$

where l are the angular momentum quantum numbers of the surface modes. The result for typical trap parameters is a critical linear velocity v_c slightly smaller than the speed of sound in the center of the trap c [23]. As we shall see, this simple analysis is not sufficient for the two kinds of geometry studied in the present paper, but needs to be modified in different ways.

III. VORTEX CREATION IN A ROTATING ANISOTROPIC POTENTIAL

Refs. [2, 8] describe experiments performed on a Bose-Einstein condensed cloud contained in a harmonic-oscillator potential that has a small ellipticity ϵ in the x - y plane which rotates with an angular frequency Ω . The time dependent potential can be written

$$V(x, y, t) = \frac{1}{2}m\omega^2 \left[(1 + \epsilon)X(t)^2 + (1 - \epsilon)Y(t)^2 \right], \quad (6)$$

where the coordinates along the corotating axes vary in time as

$$X(t) = x \cos \Omega t + y \sin \Omega t, \quad Y(t) = y \cos \Omega t - x \sin \Omega t. \quad (7)$$

The twofold symmetric potential can only excite modes of quadrupolar symmetry. Therefore the Landau criterion, Eq. (5), must be modified so that the summation is restricted to quadrupolar modes, resulting in the criterion

$$\Omega_c = \frac{\omega_2}{2}, \quad (8)$$

where ω_2 is the excitation frequency of the lowest-lying quadrupole mode. In the Thomas-Fermi limit it is known to have the value $\omega_2 = \sqrt{2}\omega$ and therefore the Landau-criterion critical frequency for this trap geometry is $\Omega_c = \omega/\sqrt{2} \approx 0.71\omega$. However, in order for vortices to be formed, a necessary condition is not only that the quadrupole mode is excited, but also that it is unstable [9, 10]. This has been shown to occur when the ellipticity is larger than the critical value

$$\epsilon_0 = \frac{2\omega}{\Omega} \left(\frac{2(\Omega/\omega)^2 - 1}{3} \right)^{2/3}. \quad (9)$$

The onset of instability above the quadrupole frequency has been investigated in detail in Ref. [11]. In Ref. [8], it was found experimentally that vortices were indeed created only for $\epsilon > \epsilon_0$ when $\Omega > \omega/\sqrt{2}$. On the other hand, for driving frequencies slower than the

quadrupole frequency, vortices could still be created if the ellipticity exceeded a Ω -dependent value that appears to be well approximated by the straight line $\epsilon = 0.71 - \Omega/\omega$. This can be thought of as a finite width of the resonance at $\Omega = \omega/\sqrt{2}$. In Ref. [8] it was speculated that this finite width is either due to finite temperature or the excitation of surface modes with higher multipolarity $m > 2$. The former proposition seems unlikely because there was little temperature variation of the position of the lower threshold value. In addition, the experimentally found sub-resonance vortex nucleation is reproduced by the zero-temperature theory of Ref. [24], as well as by the present numerics, as we shall see. Reference [24] puts up a pictorial model of vortex entry that focuses on the path taken by a vortex moving into a BEC cloud. The finite energy barrier that a vortex would have to overcome in order to move into a cylindrically symmetric cloud, even under external rotation, is found to be lowered if the cloud is elongated. The critical frequency Ω is determined by the requirement that the energy at the saddle point which the vortex has to overcome is lower than the energy of a cylindrical, nonrotating cloud. The analysis thus applies to the case of a sudden switch-on of the rotation. The critical frequency is shifted down from the quadrupole frequency by an amount that depends on both ϵ and the coupling strength. However, in the case of an adiabatically slow increase of the rotational force, the model of Ref. [24] would predict no vortex entry, because there will always be a local energy minimum for a vortex-free elongated state and therefore a finite energy barrier for a vortex to overcome.

The numerical procedure mimics the experimental conditions of Ref. [8], which has an effective two-dimensional coupling strength $Na/l_z = 56$. The two-dimensional calculation neglects any degrees of freedom associated with the z direction, which is a valid approximation since the experimental trap is oblate with an aspect ratio $\omega/\omega_z \approx 0.35$ and in such a trap vortices are expected to be straight [25, 26]. The cloud is initially taken to be in equilibrium in a stationary trap with zero ellipticity in the x - y plane. The ellipticity ϵ is ramped up from zero to its final value over a time $t_{\text{init}} = 80 \omega^{-1}$ while the rotation frequency Ω is held constant. The subsequent evolution is monitored for another $300 \omega^{-1}$; typically the vortex nucleation starts after a time comparable to the ramping-up time when Ω lies above the quadrupole frequency. To obtain a diagnostics for the presence of vortices, the ellipticity is subsequently ramped down between $t = 300 \omega^{-1}$ and $t = 380 \omega^{-1}$, whereafter the vorticity in an area enclosed by a circle of radius R_{TF} is computed and averaged over a time span of $100 \omega^{-1}$ in the cylindrically symmetric trap. An average vorticity above 0.3 is

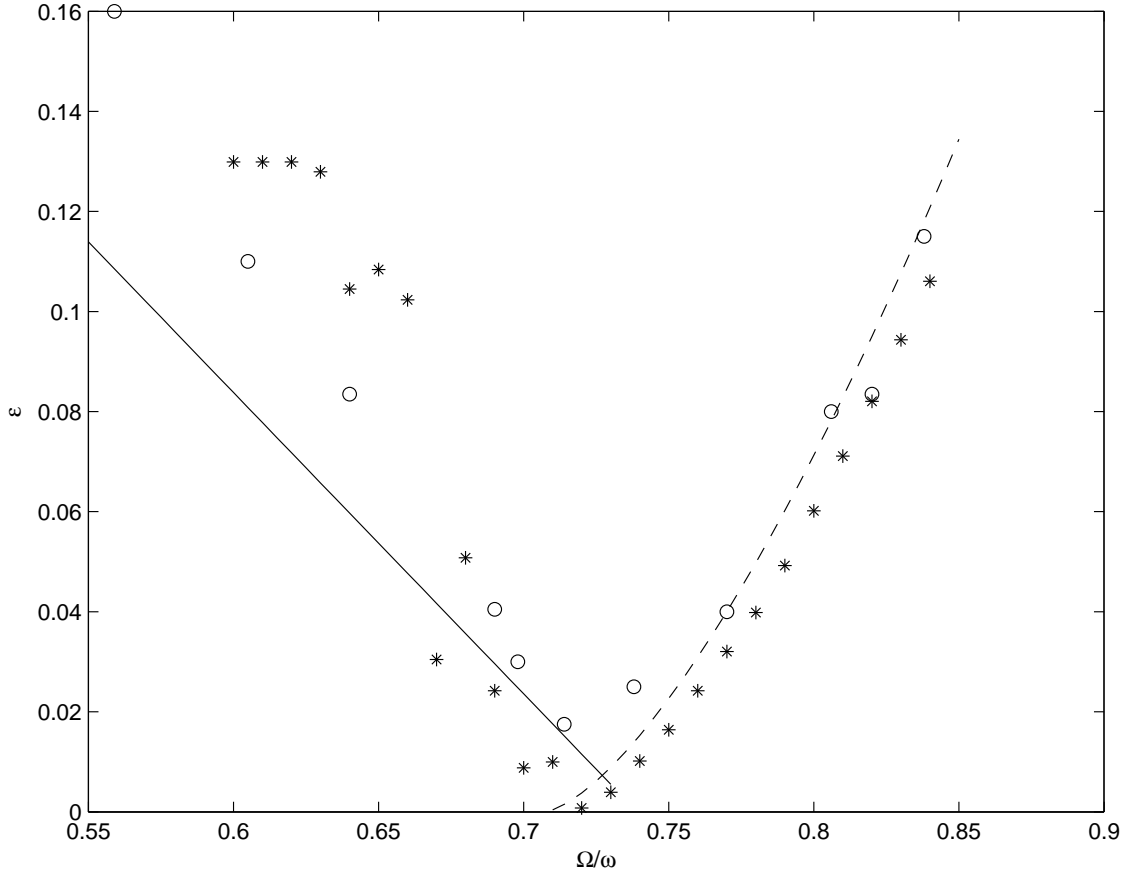


FIG. 1: Critical values of the anisotropy ϵ of a rotating anisotropic trap for the onset of vortex nucleation. Asterisks denote the numerical results from solving the Gross-Pitaevskii equation, the dashed line is the analytical prediction of Ref. [9], and the circles represent the experimental results of Ref. [8]. The solid line represents the analytical estimate of Ref. [24], which is a theory for sudden switch-on of the rotation, applied to the case of a chemical potential $\mu = 12\hbar\omega$.

taken to be indicative of the fact that vortices spend a nonnegligible time in the interior of the cloud; the results are not sensitive to the precise threshold value.

Figure 1 shows the critical value of ϵ as a function of Ω . It is seen that the numerical results are in good agreement with the experimental findings and the theory of Ref. [9] when Ω is larger than the quadrupole frequency, but the agreement is somewhat poorer below. The qualitative features are, however, well captured by our numerics. This fact rules out the possibility that vortex excitation below the quadrupole frequency is purely a finite-temperature effect, since the present study is performed using zero-temperature theory.

The prediction by Ref. [24] is also in rough agreement with the experiment and the present

numerics but predicts a lower critical anisotropy, which is expected since it applies to the case of a sudden switch-on of the trap. We speculate that the present ramping-up time, although long compared to the period of the forcing Ω^{-1} , is still not perfectly adiabatic. While the threshold values of ϵ and Ω agree with the experimental findings of Ref. [8], the observed numbers of vortices turn out to be somewhat higher. This can be due to lack of equilibration or because our numerical counting method includes vortices on the edge of the condensate that are not visible to the eye.

In order to better understand the transition to the vortex state, we study in detail the evolution of the z component of the angular momentum L_z and the mean extension of the cloud along two axes corotating with the trap, $X_{\text{rms}} = \sqrt{\langle X^2 \rangle}$ and $Y_{\text{rms}} = \sqrt{\langle Y^2 \rangle}$. The deformation of the cloud is denoted δ and defined as

$$\delta = \frac{Y_{\text{rms}}^2 - X_{\text{rms}}^2}{Y_{\text{rms}}^2 + X_{\text{rms}}^2}, \quad (10)$$

in accordance with Ref. [24]. In Fig. 2, these four quantities, together with the vorticity N_v in an area enclosed by a circle of radius R_{TF} are plotted against time for the choice of parameters $\Omega = 0.78\omega$ and $\epsilon = 0.1$. This point lies in the right part of the phase diagram of Fig. 1, above the quadrupole frequency; we shall soon comment on the difference in behavior for different Ω . In this plot, the anisotropy ϵ is initially ramped up for a time $t = 80\omega^{-1}$ as before, but is then held constant throughout the simulation in order to display the physics more clearly. We see how the cloud is initially elongated and at the same time rotates with the trap. The cloud initially rotates 90 degrees out of phase with the potential, so that the elongation is in the direction of stronger trapping potential, consistent with Ref. [8]. The elongation of the cloud would now begin to oscillate around an equilibrium value if the frequency and ellipticity were outside the critical region. Within the critical region, the maximum elongation instead grows larger until the outer edges of the cloud bend, close in on themselves, and capture vortices; the first vortex is seen to be detected just prior to $t = 50\omega^{-1}$ when the cloud elongation is at its largest. After a turbulent period, the anisotropy of the cloud is somewhat decreased. During and after vortex capture, the orientation of the cloud is changed so that the elongation is in the direction of weaker trapping. The whole process is in accordance with previously reported results [2, 8, 9, 10]. We do not observe an actual crystallization of the vortices into a lattice during the waiting time allowed for here. A recent preprint suggests that the crystallization of a lattice should occur even at zero temperature

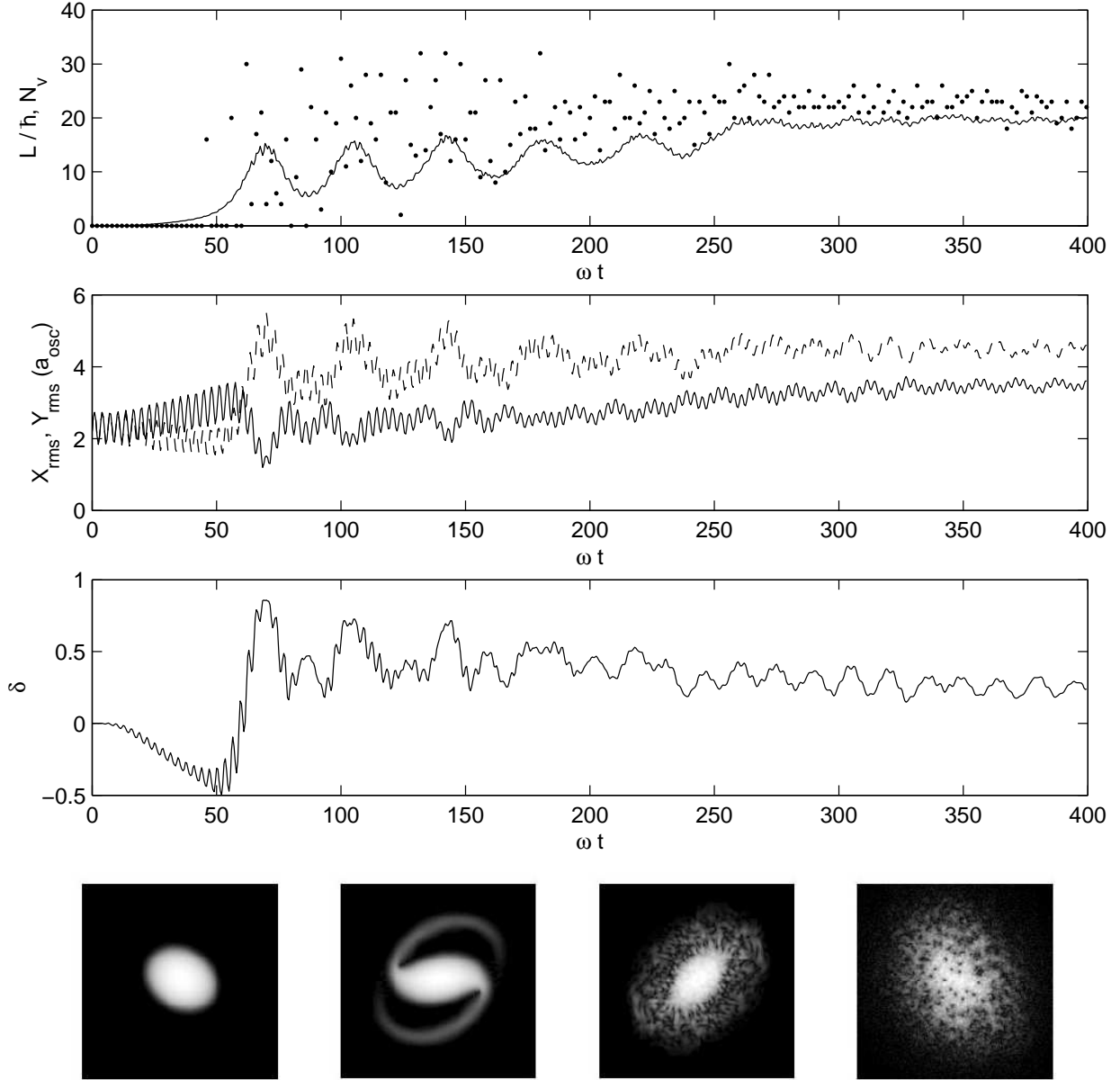


FIG. 2: The upper panel shows the time evolution of the angular momentum (full curve) and number of vortices N_v (dots) in a trap with an anisotropy $\epsilon = 0.1$ rotated at a frequency $\Omega = 0.78\omega$. The second panel from the top is a plot of the rms radii of the cloud along two axes corotating with the anisotropic trap: the full curve describes $X_{\text{rms}} = \sqrt{\langle X^2 \rangle}$ and the dashed curve describes $Y_{\text{rms}} = \sqrt{\langle Y^2 \rangle}$. The third panel depicts the dimensionless cloud deformation δ as a function of time. The four pictures on the bottom are density plots taken at the time instances $t = 27\omega^{-1}$, $t = 80\omega^{-1}$, $t = 160\omega^{-1}$, and $t = 400\omega^{-1}$, respectively. Brighter shades represent higher density.

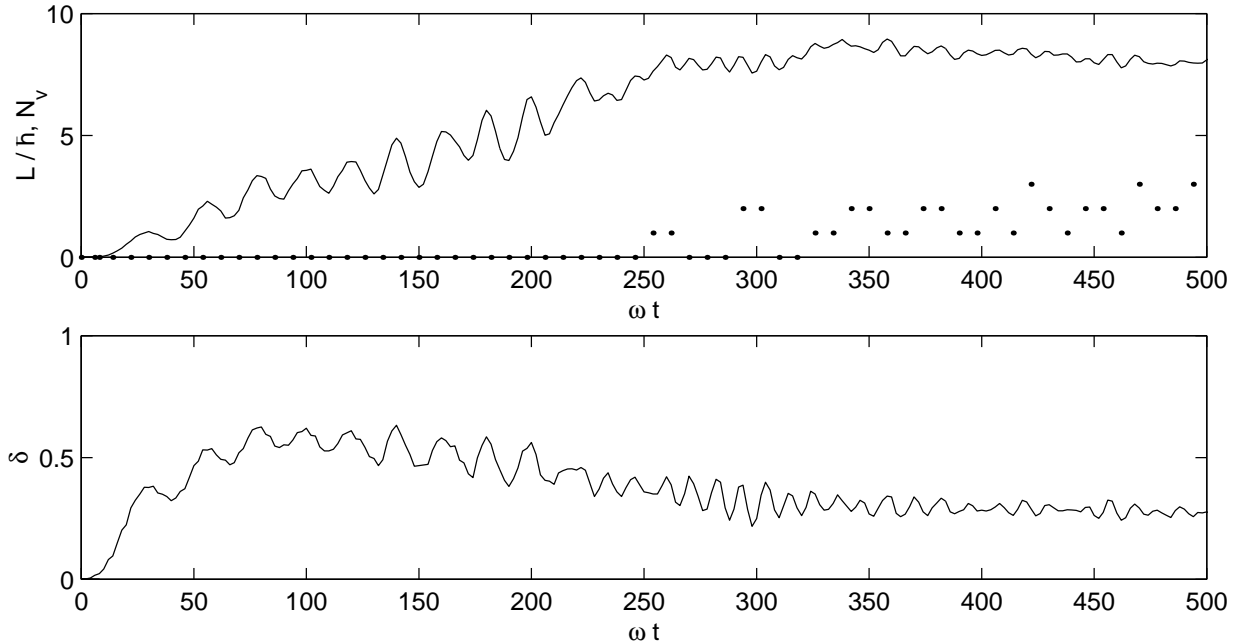


FIG. 3: The upper panel shows the time evolution of the angular momentum (full curve) and number of vortices N_v (dots) in a trap with an anisotropy $\epsilon = 0.2$ rotated at a frequency $\Omega = 0.64\omega$. The lower panel depicts the dimensionless cloud deformation δ as a function of time.

[19], but the difference in dimensionality, trap geometry and number of vortices prevents a quantitative comparison of the time scales. The effect of dissipative mechanisms on the lattice formation was studied in Refs. [17, 18].

Below the quadrupole frequency, the process is markedly different. Fig. 3 depicts the evolution of the angular momentum, vorticity, and cloud deformation δ in this regime. The cloud is initially elongated, but the elongation of the cloud rotates in phase with the trap deformation so that δ is positive. The cloud deformation is seen to grow to a maximum whereafter vortices enter the cloud, consistent with the physical picture of Ref. [24]. The buildup of angular momentum takes place gradually and smoothly compared with the situation in Fig. 2.

Figure 4 displays the time evolution of the angular momentum for two different choices of Ω , providing representative examples of the evolution of angular momentum below and above the critical line. Clearly, the physics of the vortex creation is different depending on whether the rotation frequency is larger or smaller than the quadrupole frequency. Above the quadrupole frequency (rightmost panel in Fig. 4), the vortex formation is very fast, and

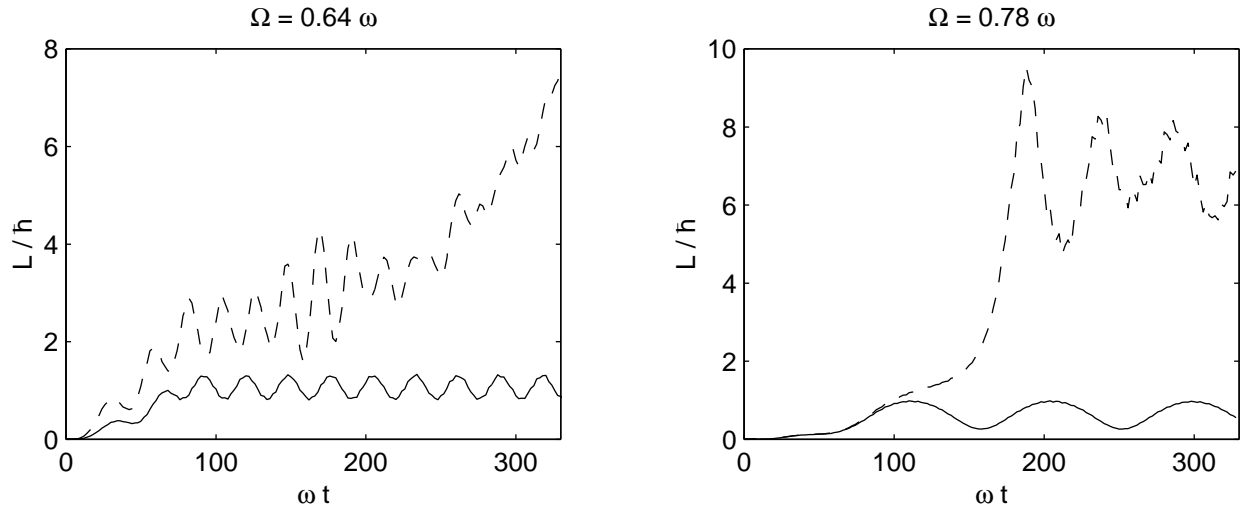


FIG. 4: Time evolution of the angular momentum in a rotating anisotropic trap for different values of the rotation frequency Ω and trap anisotropy ϵ . In the left panel, the rotation frequency $\Omega = 0.64\omega$ and the trap deformation $\epsilon = 0.1$ (full line) and $\epsilon = 0.17$ (dashed line). In the right panel, the rotation frequency $\Omega = 0.78\omega$ and the trap deformation $\epsilon = 0.41$ (full line) and $\epsilon = 0.42$ (dashed line). For the solid lines, the parameter values are such that no vortices are created, while the oscillations in the case of the dashed lines are associated with vortex creation.

the oscillations in the vortex-free regime are distinct from the turbulent behavior leading to vortex formation, although the values of ϵ for the dashed and full curves differ by a very small amount. Below the quadrupole frequency, however, vortex formation is preceded by a gradual buildup of angular momentum, and the outgrowth of “arms” from the cloud seems to be absent. In this regime, it takes a finite time for the instability associated with vortex formation to occur.

The critical lines can thus be determined with good accuracy above the quadrupole frequency, but below the quadrupole frequency, they have a more pronounced dependence on the waiting time. This fact together with the turbulent fluid flow and sensitivity to details that is connected with the vortex creation is the reason for the scatter of the numerical data points in Fig. 1. The gradual buildup of vorticity is consistent with the view that vortices enter the cloud only when there is an appreciable elongation (or equivalently, population of the quadrupole mode); this cannot be captured by the linear stability analysis of Ref. [10]. An alternative, but probably equivalent picture, is the one proposed in Ref. [24], which still holds if the rotation is switched on moderately rapidly. Another possibility could be that the

vortex creation is dependent on the excitation of higher than quadrupolar modes due to trap imperfections (which in the simulations would then be due to the square numerical grid). But if this were the case, we would not have expected the fair quantitative agreement between numerics and experiment that is after all visible in Fig. 1. (The occupation of modes during vortex nucleation has been studied numerically in Ref. [18], but without special attention to the difference between frequencies below and above the quadrupole frequency.) We therefore conclude that the cause for vortex excitation in this regime is not to be found in factors extrinsic to the zero-temperature Gross-Pitaevskii equation.

IV. STIRRING A CONDENSATE WITH A LOCALIZED POTENTIAL

In the experiment reported in Ref. [12], angular momentum was imparted to the condensate by stirring it with a pair of narrow repulsive laser beams, placed opposite to each other and rotating about the center at a radius r_s with an angular frequency Ω , so that the linear velocity is $v_s = \Omega r_s$. The vortex formation is in this case governed by quite different physics compared to the previous section. In fact, there exists a crossover: in the limit of a pair of wide beams at large r_s , the potential becomes again that of a rotating anisotropic trap and the analysis of the previous section applies. Here we shall, however, study the case of narrow beams at both large and small distances from the center. We take the potential to be a harmonic-oscillator one plus two symmetrically placed repulsive Gaussian “sticks” revolving about the origin:

$$V(x, y) = \frac{1}{2}m\omega^2(x^2 + y^2) + V_0 \left(e^{-\frac{|\mathbf{r}-\mathbf{r}_0(t)|^2}{2\sigma^2}} + e^{-\frac{|\mathbf{r}+\mathbf{r}_0(t)|^2}{2\sigma^2}} \right). \quad (11)$$

The stirrer coordinates are given by $\mathbf{r}_0(t) = (x_0(t), y_0(t))$ with

$$\begin{aligned} x_0(t) &= r_s \cos \Omega t, \\ y_0(t) &= r_s \sin \Omega t, \end{aligned} \quad (12)$$

and the stirrer width σ is smaller than the cloud size R_{TF} but not smaller than the healing length ξ . We have chosen to consistently work with a pair of stirrers in order to facilitate comparison with the experimental data of Ref. [12]. We have, however, found no qualitative differences when comparing with test runs made with one stirrer.

The physics of the vortex creation is the following [13]. When an object or a repulsive potential is moved through the condensate, pairs of vortices with unit positive and negative

circulation are created in the wake. Positively oriented vortices will be created to the left of the stirrer relative to its direction of movement, and negatively oriented vortices, antivortices, to the right. (This can be realized by considering how the fluid flows back around the stirrer to fill the wake.) The vortices and antivortices follow the local current which initially is directed at an oblique angle, away from the stirrer and in the direction of movement. The antivortices will quickly drift out of the system while the positive vortices may enter into the cloud depending on whether they have enough energy to do so (assuming that the stirrer rotates counterclockwise around the center; otherwise the role of vortices and antivortices is interchanged). The whole process is turbulent and is complicated by inter-vortex interaction, sound waves and density variations.

The conditions for vortex creation are thus twofold: the linear velocity of the stirrer must be large enough to create vortices, and the angular velocity of the stirrer must be large enough to contain the vortices in the interior of the cloud. We study first the former requirement. Vortex pairs are only created when the stirrer velocity exceeds a critical value given by the Landau criterion, Eq. (5). For the situation in Ref. [12], the prediction of Ref. [23] is $v_c = 0.24c$. However, this analysis was carried out for a stirrer that moves close to the edge of the condensate. For the case of a Gaussian stirrer that moves in the bulk of the condensate, the abrupt potential gradient is expected to result in a lower critical velocity v_c than that given by the surface-mode calculation [27]. In this case, a critical velocity about an order of magnitude smaller than the sound velocity c has been observed numerically [28] and experimentally [12, 29]. An approach that inserts the calculated energy and momentum of a vortex pair into the Landau criterion, Eq. (5), has yielded a critical velocity of the correct magnitude [30].

We have numerically investigated the critical velocity for the case when the coupling parameter $Na/a_{\text{osc}} = 56$, giving a Thomas-Fermi radius $R_{\text{TF}} = 5.5 a_{\text{osc}}$, and a stirrer moving at a radius $r_s = 0.2 R_{\text{TF}}$ from the center. When the stirrer size $\sigma = 0.05 R_{\text{TF}}$, the critical velocity $v_c \approx 0.45c$ and when $\sigma = 0.1 R_{\text{TF}}$, $v_c \approx 0.35c$. Due to the noisy character of the data, the error bars on the observed critical velocities are about $\pm 0.1c$. This critical velocity is larger than that of Ref. [12], but the difference in coupling strength is quite drastic: due to numerical constraints we have chosen to operate with a coupling strength Na/l_z that is smaller than that of Ref. [12] by approximately a factor 10.

When the stirrer velocity is well above the critical one so that the number of vortices

is large, the build-up of angular momentum resulting from the complex process of vortex creation and entry can be described classically. The torque exerted on the fluid by the moving disturbance is estimated as follows. Assuming that the stirring potential V_0 is strong enough, the fluid that is instantaneously right in front of it is accelerated to the velocity of the stirrer v_s . The momentum increase per unit time due to one stirrer is therefore equal to the product of the mass of the fluid occupying an area swept out by the stirrer in unit time and the increase in velocity of the fluid at radius r_s :

$$\frac{dp}{dt} = 2\sigma v_s m n_{2D}(r_s)(v_s - v(r_s)), \quad (13)$$

where $n_{2D}(r)$ is the two-dimensional density of the fluid; $n_{2D}(r) = n_{3D}(r)l_z$. The width of the stirrer is taken to be 2σ . The momentum increase is azimuthally directed, and therefore the torque acting on the gas is r_s times the quantity on the right-hand side of Eq. (13). When two stirrers are used, the momentum increase is doubled and the total torque is

$$\tau = 2 \cdot 2\sigma v_s r_s m (v_s - v(r_s)) n_{2D}(r_s). \quad (14)$$

The effect of the ensuing turbulent behavior, including the creation of vortex pairs, is to quickly distribute the momentum over the whole cloud, and when the number of vortices is large, the fluid rotates on average as a solid body: $v(r) = \omega r$. We can assume that the redistribution of momentum happens instantaneously, because the characteristic timescale for the spreading of the disturbances is $t_{\text{spread}} = R_{\text{TF}}/c$. For realistic parameter values, this timescale is indeed much shorter than the timescale for the growth of the angular momentum, and therefore the system can at all times be assumed to be in solid-body rotation. However, during the stirring, we do not expect the vortex array to extend outside the radius r_s of the stirrer. Outside the region enclosed by the path of the stirrer, the fluid velocity is the sum of velocity fields from the individual quantized vortices, decaying as the inverse distance from the vortex. A reasonable assumption for the instantaneous fluid velocity is therefore

$$v(r) = \begin{cases} \omega(t)r, & r < r_s; \\ \frac{\omega(t)r_s^2}{r}, & r > r_s, \end{cases} \quad (15)$$

where the instantaneous solid-body rotation frequency $\omega(t)$ characterizes the rotation rate. Multiplying the local velocity, Eq. (15), with r and the Thomas-Fermi density, Eq. (3), and integrating over the whole cloud, one obtains the total angular momentum per particle at

time t ,

$$L(t) = m\omega(t)r_s^2 F\left(\frac{r_s}{R_{\text{TF}}}\right), \quad (16)$$

where the function $F(x) = 1 - x^2 + x^4/3$. The derivative of the angular momentum is to be equated to the torque, Eq. (14), and the substitution of the angular momentum L for the fluid velocity $v(r_s)$ according to Eq. (16) results in

$$\dot{L} = 2\frac{2\sigma v_s n_{2D}(r_s)}{F(r_s/R_{\text{TF}})} (mr_s v_s F(r_s/R_{\text{TF}}) - L). \quad (17)$$

Solving Eq. (17) for $L(t)$, one obtains the time dependence

$$L(t) = L_{\text{fin}} (1 - e^{-2Rt}), \quad (18)$$

where the final angular velocity is

$$L_{\text{fin}} = mr_s v_s \left(1 - \left(\frac{r_s}{R_{\text{TF}}}\right)^2 + \frac{1}{3} \left(\frac{r_s}{R_{\text{TF}}}\right)^4\right), \quad (19)$$

and the rate constant:

$$R = \frac{2\sigma v_s n_{2D}(r_s)}{F(r_s/R_{\text{TF}})}. \quad (20)$$

The factor 2 multiplying the rate constant in Eq. (18) is again the factor that reflects the number of stirrers. The torque is given by

$$\tau = 2 \cdot 2m\sigma r_s v_s^2 n_{(2D)}(r_s) e^{-2Rt}. \quad (21)$$

The maximum value of the final angular momentum L_{fin} always occurs when $r_s/R_{\text{TF}} = \sqrt{(9 - \sqrt{21})}/10 \approx 0.66$. The fact that the angular momentum is optimized when the stirrer is halfway between the center and the edge of the cloud is simply due to the fact that the linear velocity of the stirrer has been held constant. The maximum angular velocity is thus determined by a balance between on the one hand the increase in the amount of fluid that is enclosed by the path of the stirrer when r_s is increased, and on the other hand the decrease in the angular velocity Ω . If Ω is held constant instead of v_s , then the angular momentum will indeed be maximized by putting the stirrer at the edge of the condensate, as can be seen by substituting Ωr_s for v_s in Eq. (19) and differentiating.

The classical model is valid in the case when many vortices are created, so that the assumption of solid-body rotation holds. The predicted final angular momentum L_{fin} , Eq.

(19), should therefore be much larger than unity; since the stirrer radius r_s is on the order of the Thomas-Fermi radius R_{TF} , this translates to the criterion

$$\frac{v_s}{a_{\text{osc}}\omega} \gg \left(\frac{l_z}{Na}\right)^{1/4}. \quad (22)$$

The classical model is thus easily satisfied when the coupling is strong, as expected. In addition, the model is expected to break down when the stirrer is in the vicinity of the cloud radius, $r_s \approx R_{\text{TF}}$, because of the Thomas-Fermi approximation. The rate R is also ill described by the classical model when it is small; requiring $R \gg t_{\text{spread}}^{-1}$ (see below Eq. (14)), we obtain the condition

$$\left(\frac{\sigma}{a_{\text{osc}}}\right) \left(\frac{v_s}{a_{\text{osc}}\omega}\right) \gg \frac{a}{l_z} \sqrt{\frac{l_z}{Na}}. \quad (23)$$

The results of the numerical calculations are found to agree well with the classical model. Calculations have been performed on a two-dimensional system with $Na/l_z = 40$, yielding a ratio between the Thomas-Fermi radius and the healing length $R_{\text{TF}}/\xi \approx 25$, so that the Thomas-Fermi approximation is applicable. The sound velocity is $c \approx 3.6\omega a_{\text{osc}}$. The stirrer velocity has been varied between ωa_{osc} and $3\omega a_{\text{osc}}$. Fig. 5 displays the final angular momentum L_{fin} of a two-dimensional cloud as a function of r_s with fixed stirrer velocity v_s , as well as the initial growth rate R (found by fitting the data to a function of the form of Eq. (18)). An illustrative example of the variation of angular momentum with time for a particular value of r_s is displayed in Figure 6. We have chosen the parameters so that the agreement is fairly good, but not perfect. However, the qualitative appearance of the L curve is the same for all parameter values. The data is noisy because of the turbulent process, especially for the rate constant which is difficult to determine accurately, but on average it is seen to agree fairly well with Eqs. (18-20) for higher values of v_s and σ so that the conditions (22-23) are met.

The classical model is seen to describe well the experiment reported in Ref. [12], even though that experiment was performed in a prolate trap with anisotropy $\omega/\omega_z = 4.3$. For this trap, the Thomas-Fermi radius in the radial direction is $R_{\text{TF}} = 12.6a_{\text{osc}}$, and the speed of sound in the center of the trap is $c = 8.5\omega a_{\text{osc}}$, where ω and a_{osc} are the radial trap frequency and oscillator length, respectively. With a linear stirrer velocity $v_s = 0.2c$, the number of vortices N_v was recorded as a function of the stirrer radius r_s . In the limit of a large vortex density, the fluid is on the average in solid-body rotation, for which $L = \hbar N_v/3$. However, we are here operating with a relatively small number of vortices, the maximum

being about 20 vortices in the experiment. Corrections to the solid-body result may therefore be important. Indeed, by calculating the angular momentum for a triangular vortex lattice in a cylindrically symmetric Thomas-Fermi cloud for different values of the lattice constant, we find the corrected number of vortices as a function of angular momentum to be well fit by the linear relation

$$N_v \approx 3 \frac{L}{\hbar} - 6. \quad (24)$$

This formula obviously breaks down when the number of vortices is close to 1, but is accurate for $N_v \geq 10$. Inserting the numerical values into Eq. (19) and using Eq. (24) for the number of vortices, we obtain for the specific conditions of Ref. [12] the relation

$$N_v = 64x \left(1 - x^2 + \frac{1}{3}x^4 \right) - 6, \quad (25)$$

where $x = r_s/R_{\text{TF}}$. The peak value of this function (at $x = 0.66$) is approximately 20.5. This result is displayed in Fig. 7, and it is seen that the agreement is good, despite the drastic difference in geometry (prolate and two-dimensional, respectively).

V. CONCLUSIONS

The nucleation of vortices in Bose-Einstein condensed gases contained in time-dependent traps has been studied numerically for two different kinds of geometry. In the case of a rotating, deformed harmonic potential, vortices are nucleated when the anisotropy of the trap exceeds a critical value. Above the critical frequency for excitation of quadrupole modes, the numerically calculated critical anisotropy is in accordance with previous theoretical and experimental results. Below the quadrupole frequency, the numerical results are again in accordance with previous experimental results, showing that the nucleation of vortices in this regime can indeed take place at zero temperature. For a cloud stirred by a narrow moving repulsive potential, a classical model has been found to describe accurately the process of angular-momentum buildup. The classical argument is based on the fact that the velocity pattern is approximately a solid-body rotation in the interior of the system, where the density of vortices is high, but potential outside the path of the stirrer. As a result, the angular momentum approaches its final value exponentially. This model is applicable when the number of vortices is large, i. e. when the stirrer velocity and width are not too small.

Acknowledgments

The authors acknowledge stimulating discussions with David Feder. We are grateful to Eleanor Hodby and to Chandra Raman for sharing experimental data with us. We acknowledge the Academy of Finland (Project 50314) for financial support. In addition, E. L. is supported by the European Network “Cold Atoms and Ultra-precise Atomic Clocks”. J.-P. M. is supported by the Stichting voor Fundamenteel Onderzoek der Materie (FOM), which is supported by the Nederlandse Organisatie voor Wetenschappelijk Onderzoek (NWO).

-
- [1] M. R. Matthews, B. P. Anderson, P. C. Haljan, D. S. Hall, C. E. Wieman, and E. A. Cornell, *Phys. Rev. Lett.* **83**, 2498 (1999).
 - [2] K. W. Madison, F. Chevy, W. Wohlleben, and J. Dalibard, *Phys. Rev. Lett.* **84**, 806 (2000).
 - [3] J. E. Williams and M. J. Holland, *Nature* **401**, 568 (1999).
 - [4] P. C. Haljan, I. Coddington, P. Engels, and E. A. Cornell, *Phys. Rev. Lett.* **87**, 210403 (2001).
 - [5] A. E. Leanhardt, A. Görlitz, A. P. Chikkatur, D. Kielpinski, Y. Shin, D. E. Pritchard, and W. Ketterle, *Phys. Rev. Lett.* **89**, 190403 (2002).
 - [6] M. Nakahara, T. Isoshima, K. Machida, S.-I. Ogawa, and T. Ohmi, *Physica B* **284-288**, 17 (2000).
 - [7] A. E. Leanhardt, Y. Shin, D. Kielpinski, D. E. Pritchard, and W. Ketterle, e-print cond-mat/0212539 (2002).
 - [8] E. Hodby, G. Hechenblaikner, S. A. Hopkins, O. M. Maragò, and C. J. Foot, *Phys. Rev. Lett.* **88**, 010405 (2002).
 - [9] A. Recati, F. Zambelli, and S. Stringari, *Phys. Rev. Lett.* **86**, 377 (2001).
 - [10] S. Sinha and Y. Castin, *Phys. Rev. Lett.* **87**, 190402 (2001).
 - [11] K. W. Madison, F. Chevy, V. Bretin, and J. Dalibard, *Phys. Rev. Lett.* **86**, 4443 (2001).
 - [12] C. Raman, J. R. Abo-Shaeer, J. M. Vogels, K. Xu, and W. Ketterle, *Phys. Rev. Lett.* **87**, 210402 (2001).
 - [13] B. Jackson, J. F. McCann, and C. S. Adams, *Phys. Rev. Lett.* **80**, 3903 (1998).
 - [14] E. P. Gross, *Nuovo Cimento* **20**, 454 (1961).
 - [15] L. P. Pitaevskii, *Zh. Eksp. Teor. Fiz* **40**, 646 (1961) [*Sov. Phys. JETP* **13**, 451 (1961)].

- [16] G. Baym and C. J. Pethick, Phys. Rev. Lett. **76**, 6 (1996).
- [17] A. A. Penckwitt, R. J. Ballagh, and C. W. Gardiner, e-print cond-mat/0205037 (2002).
- [18] K. Kasamatsu, M. Tsubota and M. Ueda, e-print cond-mat/0211394 (2002).
- [19] C. Lobo, A. Sinatra, and Y. Castin, e-print cond-mat/0301628 (2003).
- [20] E. Lundh, C. J. Pethick, and H. Smith, Phys. Rev. A **55**, 2126 (1997).
- [21] C. J. Pethick and H. Smith, *Bose-Einstein Condensation in Dilute Gases* (Cambridge University Press, Cambridge, 2001).
- [22] D. L. Feder, C. W. Clark, and B. I. Schneider, Phys. Rev. A **61**, R011601 (1999).
- [23] J. R. Anglin, Phys. Rev. Lett. **87**, 240401 (2001).
- [24] M. Krämer, L. Pitaevskii, S. Stringari and F. Zambelli, Laser Phys. **12**, 113 (2002).
- [25] J. J. García-Ripoll and V. M. Pérez-García, Phys. Rev. A **63**, 041603 (2001).
- [26] A. Aftalion and T. Riviere, Phys. Rev. A **64**, 043611 (2001).
- [27] Preliminary calculations along the lines of Ref. [23] on the flow past a Gaussian boundary in an infinite system indicate that the critical velocity is in this case indeed much lower than in the corresponding case with a linear-ramp potential considered there.
- [28] B. Jackson, J. F. McCann, and C. S. Adams, Phys. Rev. A **61**, R051603 (2000).
- [29] R. Onofrio, C. Raman, J. M. Vogels, J. R. Abo-Shaer, A. P. Chikkatur, and W. Ketterle, Phys. Rev. Lett. **85**, 2228 (2000).
- [30] M. Crescimanno, C. G. Koay, R. Peterson, and R. Walsworth, Phys. Rev. A **62**, 063612 (2000).

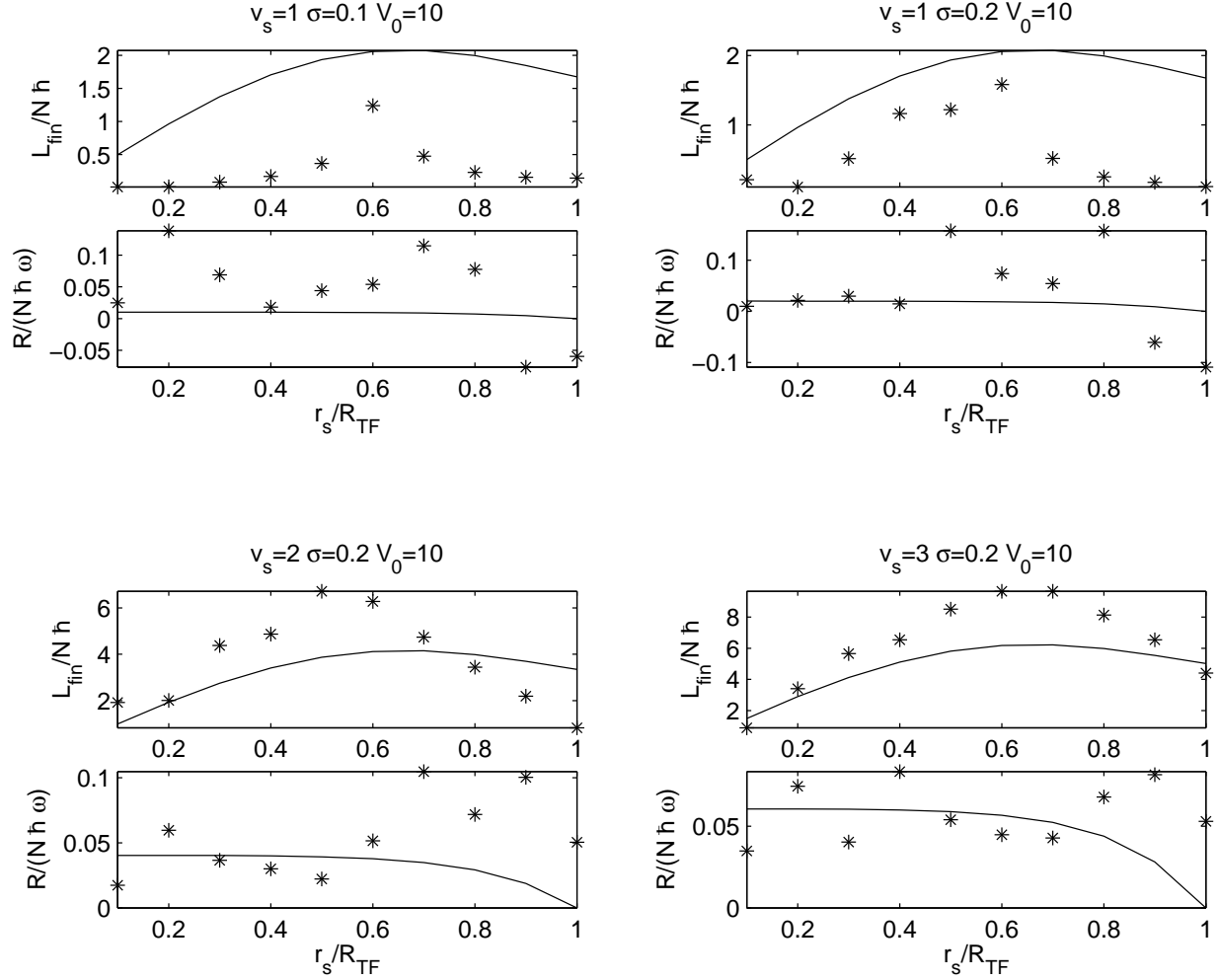


FIG. 5: Final angular momentum (upper panels) and initial rate of increase of angular momentum (lower panels) for a condensate stirred by two rotating laser beams, as functions of the distance of the stirrers from the trap center. The stirrer velocity v_s , stirrer width σ and peak stirrer potential V_0 are stated above each panel in units of the trap frequency ω , oscillator length a_{osc} , and trap energy $\hbar\omega$. The lines are the classical equations explained in the text and the asterisks connected with lines are numerical results from the two-dimensional Gross-Pitaevskii equation. The coupling strength is chosen to $Na/l_z = 40$, whereby the sound velocity $c \approx 3.6$ and Thomas-Fermi radius $R_{TF} \approx 5.0$ in trap units. The agreement with the classical prediction is best in the panels on the lower right, where the number of vortices is the largest.

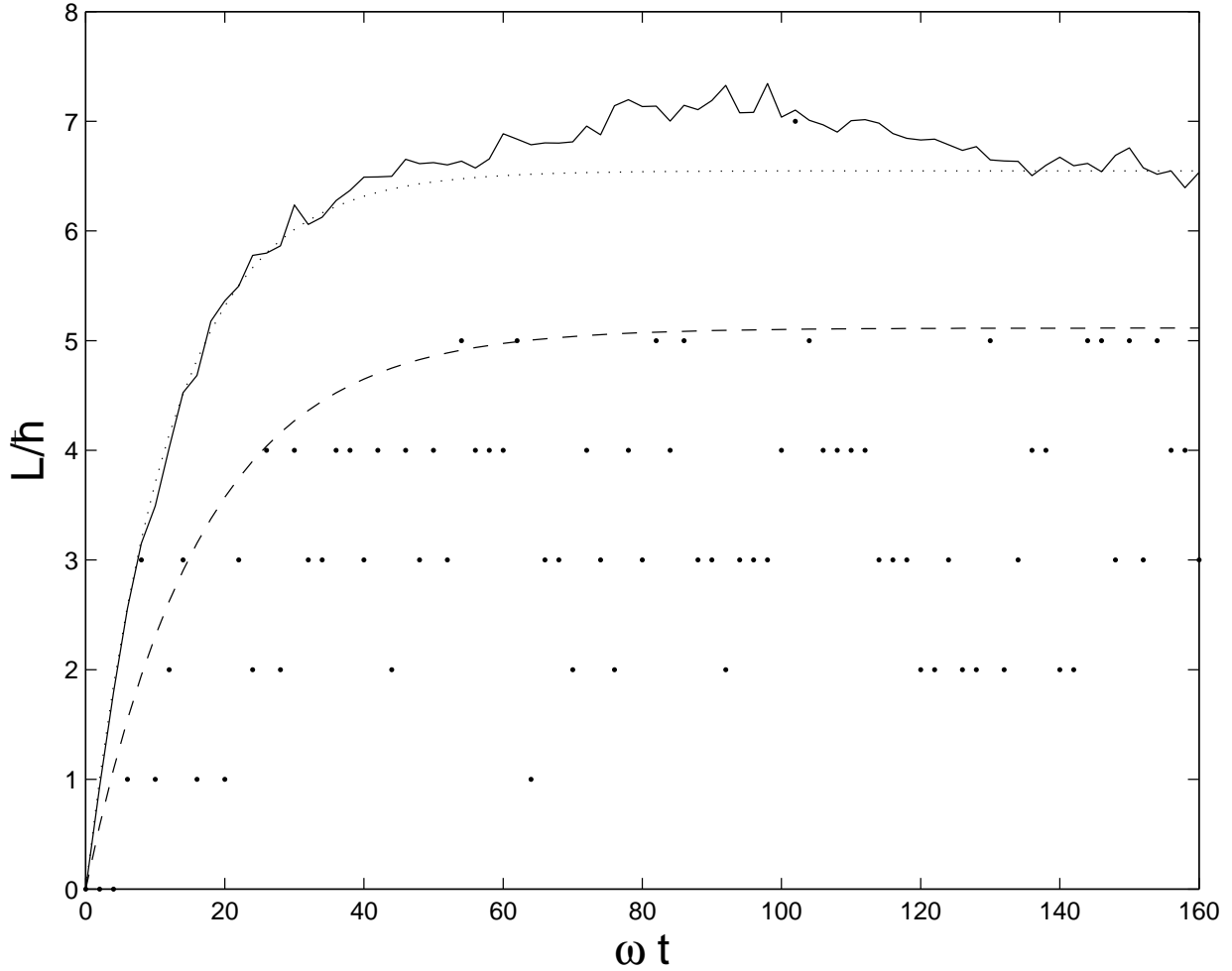


FIG. 6: Time evolution of the angular momentum and the number of vortices of a condensate stirred by two rotating laser beams. The solid line denotes the numerically computed angular momentum, the dashed line is the classical prediction, the dotted line is a fit of the solid curve to a function of the form (18), and the dots signify the number of vortices in the interior of the cloud. The parameter values are the same as in the lower left two panels of Fig. 5: $v_s = 3\omega a_{\text{osc}}$, $\sigma = 0.4a_{\text{osc}}$, and we have chosen $r_s = 0.6R_{\text{TF}}$.

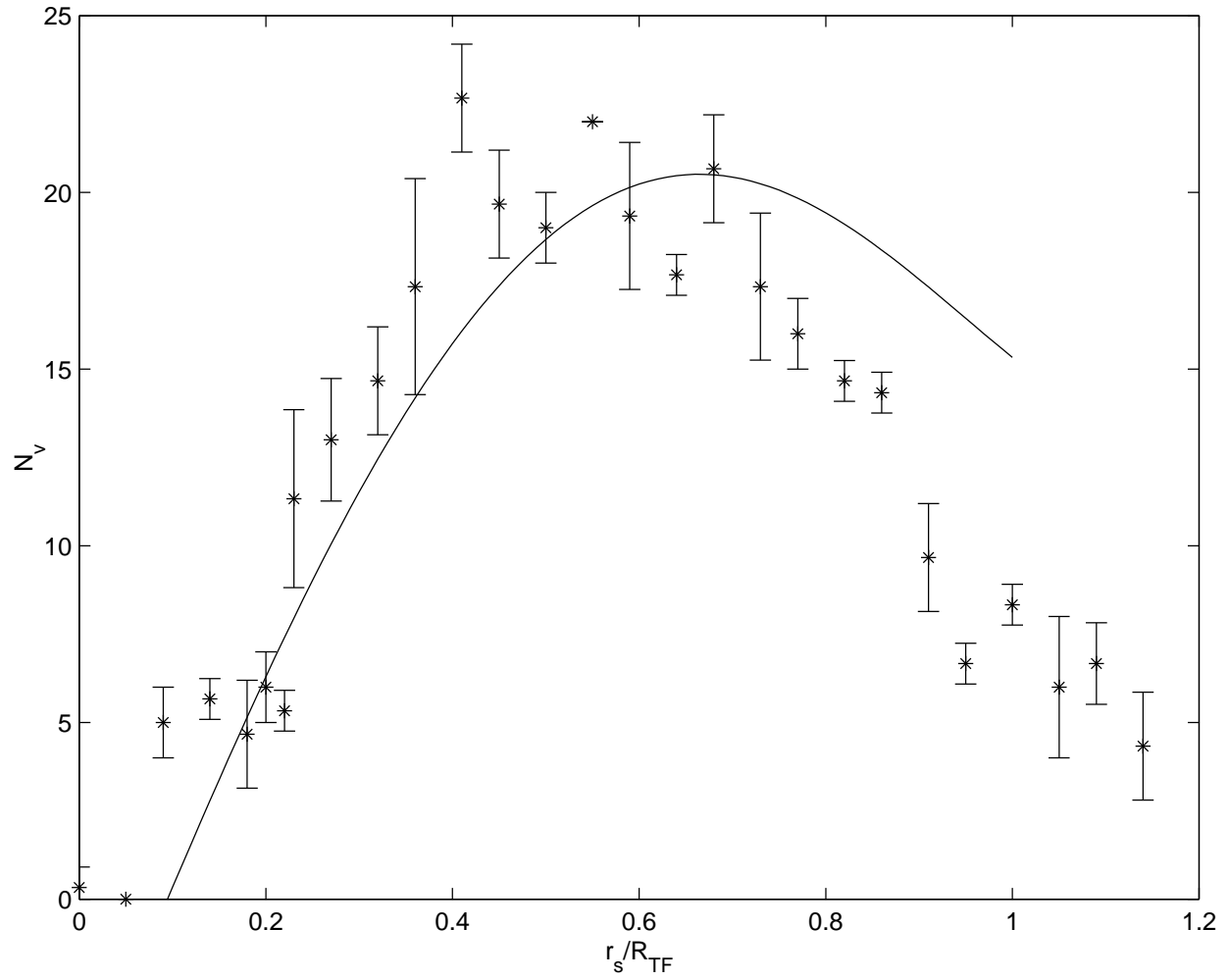


FIG. 7: Number of vortices after stirring as a function of the stirrer position for the conditions of the MIT experiment of Ref. [12]. The solid line depicts the classical model and the asterisks with error bars are the experimental results.